Advances in Applied Mathematics and Mechanics
Adv. Appl. Math. Mech., Vol. **2**, No. 2, pp. 183-199

DOI: 10.4208/aamm.09-m0962
April 2010

The Pressure-Streamfunction MFS Formulation for the Detection of an Obstacle Immersed in a Two-Dimensional Stokes Flow

A. Karageorghis[1,*] and D. Lesnic[2]

[1] *Department of Mathematics and Statistics, University of Cyprus, P.O.Box 20537, 1678 Nicosia, Cyprus*

[2] *Department of Applied Mathematics, University of Leeds, Leeds LS2 9JT, UK*

Received 17 July 2009; Accepted (in revised version) 04 December 2009
Available online 5 March 2010

Abstract. In this paper we consider a geometric inverse problem which requires detecting an unknown obstacle such as a submarine or an aquatic mine immersed in a Stokes slow viscous stationary flow of an incompressible fluid, from a single set of Cauchy (fluid velocity and stress force) boundary measurements. The numerical reconstruction is based on the method of fundamental solutions (MFS) for the pressure and streamfunction in two dimensions combined with regularization. Numerical results are presented and discussed.

AMS subject classifications: 33A65, 65N35, 65N22, 65F05, 35J05.

Key words: Stokes flow, method of fundamental solutions, regularization, streamfunction, stress force.

1 Introduction

Recently, the inverse geometric problem of detecting an immersed obstacle in a fluid via non-invasive Cauchy boundary measurements has been addressed in [2]. This inverse problem belongs to the wider class of inverse problems in fluid mechanics, namely, the detection of solid bodies such, as submarines or aquatic mines, from boundary or internal measurements in stationary flows of ideal fluids, see [1], Stokes fluids, see [3, 12, 14, 22, 26], Oseen fluids, see [21], or Navier-Stokes fluids, see [11].

*Corresponding author.
URL: `http://www.maths.leeds.ac.uk/applied/staff.dir/lesnic/lesnic.html`
Email: andreask@ucy.ac.cy (A. Karageorghis), amt5ld@maths.leeds.ac.uk (D. Lesnic)

Prior to this study, Alves and Martins [5] and Martins and Silvestre [22] recently considered the application of the MFS for the detection of immersed obstacles in two-dimensional potential and Stokes flow, respectively. In [22], the authors used the velocity-pressure formulation of the inverse problem given by

$$\Delta \boldsymbol{u} = \nabla p, \qquad \text{in} \quad \Omega \backslash \overline{D}, \tag{1.1a}$$

$$\nabla \cdot \boldsymbol{u} = 0, \qquad \text{in} \quad \Omega \backslash \overline{D}, \tag{1.1b}$$

$$\boldsymbol{u} = \boldsymbol{f}, \qquad \text{on} \quad \partial\Omega, \tag{1.1c}$$

$$\boldsymbol{t} = \boldsymbol{g}, \qquad \text{on} \quad \partial\Omega, \tag{1.1d}$$

$$\boldsymbol{u} = \boldsymbol{0}, \qquad \text{on} \quad \partial D, \tag{1.1e}$$

where $\boldsymbol{u}$ is the fluid velocity, p is the fluid pressure, $\Omega \subset \mathbb{R}^2$ is a bounded domain, $\overline{D} \subset \Omega$ is the unknown obstacle with Lipschitz boundary ∂D such that $\Omega \backslash D$ is connected,

$$\boldsymbol{t} = T\boldsymbol{n}, \tag{1.2}$$

is the stress force,

$$T = \nabla \boldsymbol{u} + (\nabla \boldsymbol{u})^{tr} - pI, \tag{1.3}$$

is the stress tensor, $\boldsymbol{n}$ is the outward unit normal to the boundary, and $\boldsymbol{f}$ and $\boldsymbol{g}$ are given functions satisfying

$$\int_{\partial\Omega} \boldsymbol{f} \cdot \boldsymbol{n}\, ds = 0.$$

In Eq. (1.1e), the no-slip velocity condition can be replaced by the zero stress force (traction) boundary condition

$$\boldsymbol{t} = \boldsymbol{0}, \quad \text{on} \quad \partial D. \tag{1.4}$$

Note that the solution of the inverse problem (1.1) is unique if

$$\boldsymbol{f} \not\equiv \boldsymbol{0},$$

i.e., the unknown obstacle D is identifiable, see [4].

In recent years, the MFS has been widely used for the solution of inverse obstacle detection problems [5, 6, 8, 20, 22] due to the simplicity with which it can be implemented and its rapid convergence properties, especially in three dimensions.

In this study, we reformulate the two-dimensional inverse problem (1.1) in terms of the streamfunction-pressure, see [25]. In this way, in the application of the MFS we use the much simpler fundamental solutions of the Laplace and biharmonic operators instead of the more complicated Stokeslets vectorial fundamental solution, [15]. Remark also that the usual streamfunction-vorticity formulation, [23], is not appropriate since the pressure is present, through the stress force $\boldsymbol{t}$, via (1.3), in the boundary condition (1.1d).

The rest of the numerical procedure for the object identification follows the regularized non-linear least-squares minimization employed in [8] and [20] for cavity identification in electrostatics.

2 Streamfunction-pressure formulation

The divergence-free velocity condition (1.1b) for incompressible two-dimensional fluid flow allows for the introduction of the scalar streamfunction ψ given by

$$\boldsymbol{u} = (u, v) = \Big(\frac{\partial \psi}{\partial y}, -\frac{\partial \psi}{\partial x}\Big). \tag{2.1}$$

Some classical manipulation of the momentum Eq. (1.1a) results in the streamfunction-pressure formulation, see [25],

$$\Delta^2 \psi = 0, \quad \Delta p = 0, \qquad \text{in} \quad \Omega \backslash \overline{D}, \tag{2.2a}$$

$$\frac{\partial p}{\partial n} = \Delta \boldsymbol{u} \cdot \boldsymbol{n} = \frac{\partial \omega}{\partial y} n_1 - \frac{\partial \omega}{\partial x} n_2, \qquad \text{on} \quad \partial\Omega \cup \partial D, \tag{2.2b}$$

where $\boldsymbol{n} = (n_1, n_2)$, and

$$\omega = \Delta \psi, \tag{2.3}$$

is the fluid vorticity. Alternatively, instead of the Neumann boundary condition (2.2b) one could use the Dirichlet boundary condition on the pressure in terms of line integrals

$$p\big(x(s), y(s)\big) = p_0 + \int_{C(s)} \Big[\frac{\partial \omega}{\partial y} dx - \frac{\partial \omega}{\partial x} dy\Big], \qquad s \in \big[0, \ell(\partial D)\big], \tag{2.4a}$$

$$p\big(x_1(s), y_1(s)\big) = p_0 + \int_{C_1(s)} \Big[\frac{\partial \omega}{\partial y} dx - \frac{\partial \omega}{\partial x} dy\Big], \qquad s \in \big[0, \ell(\partial \Omega)\big], \tag{2.4b}$$

where p_0 is an arbitrary constant, $\ell(\partial D)$ and $\ell(\partial \Omega)$ are the lengths of the closed curves ∂D and $\partial \Omega$, respectively, and

$$C(s) = \big\{\big(x(t), y(t)\big) \big| t \in [0, s]\big\}, \qquad C\big(\ell(\partial D)\big) = \partial D, \tag{2.5a}$$

$$C_1(s) = \big\{\big(x_1(t), y_1(t)\big) \big| t \in [0, s]\big\}, \qquad C\big(\ell(\partial \Omega)\big) = \partial \Omega, \tag{2.5b}$$

are their parametrizations. In order to specify p_0, one can prescribe p at a given point, say $\big(x_1(0), y_1(0)\big)$, or one can impose that

$$\int_{\partial \Omega} p ds = 0.$$

In the sequel, we impose

$$p\big(x_1(0), y_1(0)\big) = p_0 = \text{given}. \tag{2.6}$$

In terms of ψ and p, the boundary conditions (1.1c)-(1.1e) become

$$\Big(\frac{\partial \psi}{\partial y}, -\frac{\partial \psi}{\partial x}\Big) = \boldsymbol{f}, \qquad \text{on} \quad \partial \Omega, \tag{2.7a}$$

$$\Big(\Big(2\frac{\partial^2 \psi}{\partial x \partial y} - p\Big) n_1 + \Big(\frac{\partial^2 \psi}{\partial y^2} - \frac{\partial^2 \psi}{\partial x^2}\Big) n_2, \Big(\frac{\partial^2 \psi}{\partial y^2} - \frac{\partial^2 \psi}{\partial x^2}\Big) n_1 - \Big(2\frac{\partial^2 \psi}{\partial x \partial y} + p\Big) n_2\Big) = \boldsymbol{g}, \qquad \text{on} \quad \partial \Omega, \tag{2.7b}$$

$$\Big(\frac{\partial\psi}{\partial y},-\frac{\partial\psi}{\partial x}\Big)=\mathbf{0},\qquad \text{on}\quad \partial D. \tag{2.7c}$$

In order to obtain a unique solution for ψ, one also needs to specify ψ at one point on $\partial\Omega$ and one point on ∂D, say,

$$\psi\big(x_1(0),y_1(0)\big)=\psi_{\partial\Omega}=\text{given}, \tag{2.8a}$$

$$\psi\big(x(0),y(0)\big)=\psi_{\partial D}=\text{given}. \tag{2.8b}$$

3 The method of fundamental solutions (MFS)

Based on the density theorem 2.2 of Bogomolny [7], the two-dimensional biharmonic streamfunction in (2.2a) may be approximated by

$$\psi_N(\boldsymbol{x},\boldsymbol{\xi};\boldsymbol{\alpha},\boldsymbol{\beta})=A+B|\boldsymbol{x}|^2+\sum_{j=1}^{2N}\Big[\alpha_jG_2(\boldsymbol{x},\boldsymbol{\xi}_j)+\beta_jG_1(\boldsymbol{x},\boldsymbol{\xi}_j)\Big],\quad \boldsymbol{x}\in\overline{\Omega}\backslash D, \tag{3.1}$$

where $\boldsymbol{\xi}=(\boldsymbol{\xi}_j)_{j=\overline{1,N}}$ are the singularities located in D, while $\boldsymbol{\xi}=(\boldsymbol{\xi}_j)_{j=\overline{N+1,2N}}$ are the singularities located outside $\overline{\Omega}$. Also, in (3.1),

$$\boldsymbol{\alpha}=(\alpha_j)_{j=\overline{1,2N}},\quad \text{and}\quad \boldsymbol{\beta}=(\beta_j)_{j=\overline{1,2N}},$$

are unknown real coefficients to be determined by imposing boundary conditions (2.7), and

$$G_1(\boldsymbol{x},\boldsymbol{\xi}_j)=\log|\boldsymbol{x}-\boldsymbol{\xi}_j|, \tag{3.2a}$$

$$G_2(\boldsymbol{x},\boldsymbol{\xi}_j)=|\boldsymbol{x}-\boldsymbol{\xi}_j|^2\log|\boldsymbol{x}-\boldsymbol{\xi}_j|, \tag{3.2b}$$

are fundamental solutions of the Laplace and biharmonic operators, respectively. In (3.1), the constants A and B which account only for the possible occurrence of a couple of exceptional $\Gamma-$contours for the biharmonic equation, see [9], can be taken to be zero, so that (3.1) simplifies to, see [17]

$$\psi_N(\boldsymbol{x},\boldsymbol{\xi};\boldsymbol{\alpha},\boldsymbol{\beta})=\sum_{j=1}^{2N}\Big[\alpha_jG_2(\boldsymbol{x},\boldsymbol{\xi}_j)+\beta_jG_1(\boldsymbol{x},\boldsymbol{\xi}_j)\Big],\quad \boldsymbol{x}\in\overline{\Omega}\backslash D. \tag{3.3}$$

Similarly, based on the density theorem 2.1 in [7], the two-dimensional harmonic pressure in (2.2a) can be approximated as a linear combination of the form

$$p_N(\boldsymbol{x},\boldsymbol{\xi};\boldsymbol{\gamma})=C+\sum_{j=1}^{2N}\gamma_jG_1(\boldsymbol{x},\boldsymbol{\xi}_j),\quad \boldsymbol{x}\in\overline{\Omega}\backslash D. \tag{3.4}$$

Avoiding the $\Gamma-$contours for the two-dimensional Laplace equation, see [16], one may take $C=0$, so that (3.4) simplifies to

$$p_N(\boldsymbol{x},\boldsymbol{\xi};\boldsymbol{\gamma})=\sum_{j=1}^{2N}\gamma_jG_1(\boldsymbol{x},\boldsymbol{\xi}_j),\quad \boldsymbol{x}\in\overline{\Omega}\backslash D. \tag{3.5}$$

Alternative approximations for the streamfunction based on Fichera's simple layer potential representation or the Almansi representation can also be employed, see [18, 19].

3.1 Parametrization of the unknown obstacle and choice of the boundary collocation and source points

Without loss of generality, we assume that the known outer boundary $\partial\Omega$ is a circle of radius 1 (otherwise one first maps conformally the exterior of Ω onto the exterior of the unit disk). Then, the outer boundary collocation and source points can be chosen as

$$x_{N+\ell} = \big(\cos(\tilde{\vartheta}_\ell), \sin(\tilde{\vartheta}_\ell)\big), \qquad \ell = \overline{1, M}, \tag{3.6}$$

$$\xi_{N+k} = \big(R\cos(\vartheta_k), R\sin(\vartheta_k)\big), \qquad k = \overline{1, N}, \tag{3.7}$$

where

$$\tilde{\vartheta}_\ell = \frac{2\pi(\ell-1)}{M}, \qquad \ell = \overline{1, M},$$

$$\vartheta_k = \frac{2\pi(k-1)}{N}, \qquad k = \overline{1, N}, \quad \text{and} \quad R > 1,$$

is fixed. We further assume that the unknown obstacle D is a star-shaped domain with respect to the origin.

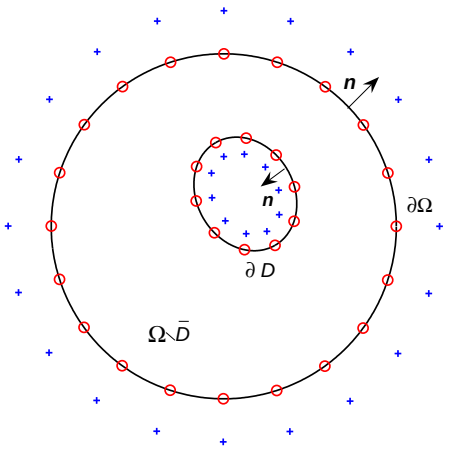

Figure 1: Geometry of the inverse problem under investigation, the MFS boundary collocation points (o) and singularities (+).

The more general case in which the center of the star-shaped domain D is unknown can also be investigated with no major modifications, see [22]. Thus we can parametrize the boundary ∂D as

$$x = r(\vartheta)\cos\vartheta, \quad y = r(\vartheta)\sin\vartheta, \quad \vartheta \in [0, 2\pi), \tag{3.8}$$

where r is a $2\pi-$periodic function. The collocation form of (3.8) in two dimensions becomes

$$r_k = r(\vartheta_k), \quad k = \overline{1,N}, \tag{3.9}$$

and we choose the inner boundary and source points as

$$\boldsymbol{x}_k = (r_k \cos\vartheta_k, r_k \sin\vartheta_k), \quad \boldsymbol{\xi}_k = \eta \boldsymbol{x}_k, \quad k = \overline{1,N}, \tag{3.10}$$

where $\eta \in (0,1)$ is fixed.

The sketch of the problem under investigation illustrating the MFS collocation points, outward unit normal vectors to the boundary, and sources is shown in Fig. 1.

3.2 Penalized least-squares minimization

The coefficients

$$(\alpha_j)_{j=\overline{1,2N}}, \quad (\beta_j)_{j=\overline{1,2N}}, \quad (\gamma_j)_{j=\overline{1,2N}}, \quad \text{and the radii } (r_j)_{j=\overline{1,N}},$$

can be determined by imposing the boundary conditions (2.2b) ($N+M$ equations), (2.6) (1 equation), (2.7a) ($2M$ equations), (2.7b) ($2M$ equations), (2.7c) ($2N$ equations), (2.8a) (1 equation) and (2.8b) (1 equation), in a least squares sense. We thus have a total of $5M+3N+3$ equations in $7N$ unknowns, which requires

$$5M+3 \geq 4N,$$

for a unique solution.

The penalized least-squares functional to be minimized is given by

$$\begin{aligned} S(\boldsymbol{\alpha},\boldsymbol{\beta},\boldsymbol{\gamma},\boldsymbol{r}) = & \sum_{j=N+1}^{N+M} \left| \left(\frac{\partial \psi_N}{\partial y}, -\frac{\partial \psi_N}{\partial x}\right)(\boldsymbol{x}_j,\boldsymbol{\xi};\boldsymbol{\alpha},\boldsymbol{\beta}) - \boldsymbol{f}(\boldsymbol{x}_j) \right|^2 + \sum_{j=N+1}^{N+M} \left| \boldsymbol{t}(\boldsymbol{x}_j,\boldsymbol{\xi};\boldsymbol{\alpha},\boldsymbol{\beta},\boldsymbol{\gamma}) \right. \\ & \left. - \boldsymbol{g}^{\varepsilon}(\boldsymbol{x}_j) \right|^2 + \sum_{j=1}^{N} \left| \left(\frac{\partial \psi_N}{\partial y}, -\frac{\partial \psi_N}{\partial x}\right)(\boldsymbol{x}_j,\boldsymbol{\xi};\boldsymbol{\alpha},\boldsymbol{\beta}) \right|^2 + \sum_{j=1}^{N+M} \left| \frac{\partial p_N}{\partial n}(\boldsymbol{x}_j,\boldsymbol{\xi};\boldsymbol{\gamma}) \right. \\ & \left. - \left(n_1(\boldsymbol{x}_j) \frac{\partial(\Delta\psi_N)}{\partial y}(\boldsymbol{x}_j,\boldsymbol{\xi};\boldsymbol{\alpha},\boldsymbol{\beta}) - n_2(\boldsymbol{x}_j) \frac{\partial(\Delta\psi_N)}{\partial x}(\boldsymbol{x}_j,\boldsymbol{\xi};\boldsymbol{\alpha},\boldsymbol{\beta}) \right) \right|^2 \\ & + \left(p_N((1,0),\boldsymbol{\xi};\boldsymbol{\gamma}) - p_0 \right)^2 + \left(\psi_N((1,0),\boldsymbol{\xi};\boldsymbol{\alpha},\boldsymbol{\beta}) - \psi_{\partial\Omega} \right)^2 \\ & + \left(\psi_N((r_1,0),\boldsymbol{\xi};\boldsymbol{\alpha},\boldsymbol{\beta}) - \psi_{\partial D} \right)^2 + \lambda_1 \left(|\alpha|^2 + |\beta|^2 + |\gamma|^2 \right) + \lambda_2 |\boldsymbol{r}|^2, \end{aligned} \tag{3.11}$$

where

(i) $\lambda_1,\ \lambda_2 \geq 0$ are regularization parameters to be prescribed in order to stabilize the numerical solution;

(ii)

$$\big(n_1(\boldsymbol{x}_j), n_2(\boldsymbol{x}_j)\big) = \begin{cases} (\cos\tilde{\vartheta}_j, \sin\tilde{\vartheta}_j), & j = \overline{N+1, N+M}, \\ \dfrac{1}{\sqrt{r_j^2 + r_j'^2}}(-r_j' \sin\vartheta_j - r_j\cos\vartheta_j, & \\ \qquad r_j'\cos\vartheta_j - r_j\sin\vartheta_j), & j = \overline{1, N}, \end{cases} \tag{3.12}$$

where

$$r_j' = r'(\vartheta_j) \approx \frac{r_{j+1} - r_{j-1}}{\vartheta_{j+1} - \vartheta_{j-1}}, \quad j = \overline{1, N},$$

with the convention

$$r_{N+1} = r_1, \quad r_0 = r_N, \quad \vartheta_{N+1} = 0, \quad \text{and} \quad \vartheta_0 = 2\pi;$$

(iii) for $j = \overline{N+1, N+M}$,

$$t_1(\boldsymbol{x}_j, \boldsymbol{\xi}; \boldsymbol{\alpha}, \boldsymbol{\beta}, \boldsymbol{\gamma}) = n_1(\boldsymbol{x}_j)\Big(2\frac{\partial^2\psi_N}{\partial x\partial y}(\boldsymbol{x}_j, \boldsymbol{\xi}; \boldsymbol{\alpha}, \boldsymbol{\beta}) - p_N(\boldsymbol{x}_j, \boldsymbol{\xi}; \boldsymbol{\gamma})\Big) + n_2(\boldsymbol{x}_j)\Big(\frac{\partial^2\psi_N}{\partial y^2} - \frac{\partial^2\psi_N}{\partial x^2}\Big)(\boldsymbol{x}_j, \boldsymbol{\xi}; \boldsymbol{\alpha}, \boldsymbol{\beta}), \tag{3.13a}$$

$$t_2(\boldsymbol{x}_j, \boldsymbol{\xi}; \boldsymbol{\alpha}, \boldsymbol{\beta}, \boldsymbol{\gamma}) = n_1(\boldsymbol{x}_j)\Big(\frac{\partial^2\psi_N}{\partial y^2} - \frac{\partial^2\psi_N}{\partial x^2}\Big)(\boldsymbol{x}_j, \boldsymbol{\xi}; \boldsymbol{\alpha}, \boldsymbol{\beta}) + n_2(\boldsymbol{x}_j)\Big(2\frac{\partial^2\psi_N}{\partial x\partial y}(\boldsymbol{x}_j, \boldsymbol{\xi}; \boldsymbol{\alpha}, \boldsymbol{\beta}) + p_N(\boldsymbol{x}_j, \boldsymbol{\xi}; \boldsymbol{\gamma})\Big); \tag{3.13b}$$

(iv) the stress force data (1.1d) comes from practical measurements which are inherently contaminated with noisy errors, and therefore we replace $\boldsymbol{g}$ by $\boldsymbol{g}^\varepsilon$ generated as

$$\boldsymbol{g}^\varepsilon(\boldsymbol{x}_j) = (1 + \rho_j\varepsilon)\boldsymbol{g}(\boldsymbol{x}_j), \quad j = \overline{N+1, N+M}, \tag{3.14}$$

where ε represents the percentage of noise and $(\rho_j)_{j=\overline{N+1,N+M}}$ are pseudo-random noisy variables drawn from a uniform distribution on $[-1, 1]$ using the NAG [24] routine `G05DAF`. Since the inverse problem under investigation is ill-posed being unstable, i.e., small errors $\varepsilon\%$ in the data (3.14) cause large errors in the solution for ∂D, the regularization term $\lambda_2|\boldsymbol{r}|^2$ has been added in order to achieve stability. Further, the regularization term

$$\lambda_1\big(|\boldsymbol{\alpha}|^2 + |\boldsymbol{\beta}|^2 + |\boldsymbol{\gamma}|^2\big),$$

has also been added in order to deal with the ill-conditioned MFS system of equations;

(v)

$$\frac{\partial\psi_N}{\partial x}(\boldsymbol{x}_j, \boldsymbol{\xi}; \boldsymbol{\alpha}, \boldsymbol{\beta}) = \sum_{k=1}^{2N}\alpha_k(x_j - \xi_k^1)\big(1 + 2\log|\boldsymbol{x}_j - \boldsymbol{\xi}_k|\big) + \sum_{k=1}^{2N}\beta_k\frac{(x_j - \xi_k^1)}{|\boldsymbol{x}_j - \boldsymbol{\xi}_k|^2}, \tag{3.15a}$$

$$\frac{\partial \psi_N}{\partial y}(\boldsymbol{x}_j,\boldsymbol{\xi};\boldsymbol{\alpha},\boldsymbol{\beta}) = \sum_{k=1}^{2N} \alpha_k (y_j-\xi_k^2)\big(1+2\log|\boldsymbol{x}_j-\boldsymbol{\xi}_k|\big) + \sum_{k=1}^{2N} \beta_k \frac{(y_j-\xi_k^2)}{|\boldsymbol{x}_j-\boldsymbol{\xi}_k|^2}, \tag{3.15b}$$

$$\frac{\partial p_N}{\partial x}(\boldsymbol{x}_j,\boldsymbol{\xi};\boldsymbol{\alpha},\boldsymbol{\beta}) = \sum_{k=1}^{2N} \gamma_k \frac{(x_j-\xi_k^1)}{|\boldsymbol{x}_j-\boldsymbol{\xi}_k|^2}, \qquad \frac{\partial p_N}{\partial y}(\boldsymbol{x}_j,\boldsymbol{\xi};\boldsymbol{\alpha},\boldsymbol{\beta}) = \sum_{k=1}^{2N} \gamma_k \frac{(y_j-\xi_k^2)}{|\boldsymbol{x}_j-\boldsymbol{\xi}_k|^2}, \tag{3.15c}$$

$$\frac{\partial^2 \psi_N}{\partial x^2}(\boldsymbol{x}_j,\boldsymbol{\xi};\boldsymbol{\alpha},\boldsymbol{\beta}) = \sum_{k=1}^{2N} \alpha_k \Big(1+2\log|\boldsymbol{x}_j-\boldsymbol{\xi}_k| + 2\frac{(x_j-\xi_k^1)^2}{|\boldsymbol{x}_j-\boldsymbol{\xi}_k|^2}\Big) + \sum_{k=1}^{2N} \beta_k \frac{(y_j-\xi_k^2)^2-(x_j-\xi_k^1)^2}{|\boldsymbol{x}_j-\boldsymbol{\xi}_k|^4}, \tag{3.15d}$$

$$\frac{\partial^2 \psi_N}{\partial y^2}(\boldsymbol{x}_j,\boldsymbol{\xi};\boldsymbol{\alpha},\boldsymbol{\beta}) = \sum_{k=1}^{2N} \alpha_k \Big(1+2\log|\boldsymbol{x}_j-\boldsymbol{\xi}_k| + 2\frac{(y_j-\xi_k^2)^2}{|\boldsymbol{x}_j-\boldsymbol{\xi}_k|^2}\Big) + \sum_{k=1}^{2N} \beta_k \frac{(x_j-\xi_k^1)^2-(y_j-\xi_k^2)^2}{|\boldsymbol{x}_j-\boldsymbol{\xi}_k|^4}, \tag{3.15e}$$

$$\Delta \psi_N(\boldsymbol{x}_j,\boldsymbol{\xi};\boldsymbol{\alpha},\boldsymbol{\beta}) = \omega_N(\boldsymbol{x}_j,\boldsymbol{\xi};\boldsymbol{\alpha},\boldsymbol{\beta}) = 4\sum_{k=1}^{2N} \alpha_k\big(1+\log|\boldsymbol{x}_j-\boldsymbol{\xi}_k|\big), \tag{3.15f}$$

$$\frac{\partial^2 \psi_N}{\partial x \partial y}(\boldsymbol{x}_j,\boldsymbol{\xi};\boldsymbol{\alpha},\boldsymbol{\beta}) = 2\sum_{k=1}^{2N} \Big[\alpha_k - \frac{\beta_k}{|\boldsymbol{x}_j-\boldsymbol{\xi}_k|^2}\Big] \frac{(x_j-\xi_k^1)(y_j-\xi_k^2)}{|\boldsymbol{x}_j-\boldsymbol{\xi}_k|^2}, \tag{3.15g}$$

$$\frac{\partial p_N}{\partial n}(\boldsymbol{x}_j,\boldsymbol{\xi};\boldsymbol{\gamma}) = \nabla p_N \cdot \boldsymbol{n} = \sum_{k=1}^{2N} \gamma_k \frac{(\boldsymbol{x}_j-\boldsymbol{\xi}_k)\cdot \boldsymbol{n}(\boldsymbol{x}_j)}{|\boldsymbol{x}_j-\boldsymbol{\xi}_k|^2}, \tag{3.15h}$$

$$\frac{\partial \omega_N}{\partial y} n_1 - \frac{\partial \omega_N}{\partial x} n_2 = 4\sum_{k=1}^{2N} \alpha_k \Big[\frac{(y_j-\xi_k^2)n_1(\boldsymbol{x}_j) - (x_j-\xi_k^1)n_2(\boldsymbol{x}_j)}{|\boldsymbol{x}_j-\boldsymbol{\xi}_k|^2}\Big], \tag{3.15i}$$

where $j = \overline{1, N+M}$, and in the above equations

$$\boldsymbol{x}_j = (x_j, y_j), \quad \text{and} \quad \boldsymbol{\xi}_k = (\xi_k^1, \xi_k^2).$$

(vi) Remark that in the direct problem (when D is known) given by Eqs. (2.2a), (2.2b), (2.6), (2.7a), (2.7c), (2.8a) and (2.8b), the functional S does not depend on $\boldsymbol{r}$ and in the expression (3.11), $\lambda_2 = 0$, and the second term (in the stress force) in the right-hand side drops out.

The minimization of (3.11) is carried out using the `MINPACK` routine `lmdif` which minimizes the unconstrained sum of squares of nonlinear functions. The constraints

$$0 < r_i < 1, \quad i = \overline{1, N},$$

are imposed during the iterative procedure by adjustment at each iteration. The Jacobian is calculated internally using forward finite differences and the minimization process terminates when either a user-specified tolerance is achieved or when a user-specified maximum number of function evaluations, `maxfev`, is reached. Thus in some cases, it is possible that the actual number of function evaluations preformed, `nfev`, is less than `maxfev`. In all numerical experiments carried out we set the tolerance to be

equal to 10^{-10}. The initial guess for the unknowns has been taken arbitrarily to be

$$\boldsymbol{\alpha}^{(0)} = \boldsymbol{\beta}^{(0)} = \boldsymbol{\gamma}^{(0)} = \mathbf{0}, \quad \text{and} \quad \boldsymbol{r}^{(0)} = 0.3.$$

In principle, one could optimize the values of R and η in (3.7) and (3.10) by treating them as unknowns in (3.11), but this will further complicate the nonlinearity of the functional. Therefore, for simplicity, we have decided to fix the values of R and η to 2 and 0.5, respectively. The results obtained with other values of R and η within this order have been found to be similar.

4 Numerical examples

4.1 Example 1

We first consider an example for which an analytical solution is available in order to assess the accuracy and stability of the proposed MFS described in Section 3. In particular, we take

$$D = \left\{(x,y) \in \mathbb{R}^2 | x^2 + y^2 < R_0^2 < 1\right\}, \qquad R_0 = 0.6, \tag{4.1}$$

$$\psi(x,y) = \frac{1}{2}\left\{c_1 \log(x^2+y^2) - c_2(x^2+y^2)\right\}, \qquad (x,y) \in \overline{\Omega}\backslash D, \tag{4.2}$$

$$p(x,y) = 0, \qquad (x,y) \in \overline{\Omega}\backslash D. \tag{4.3}$$

This gives the fluid velocity

$$\boldsymbol{u} = (u,v) = \Big(\frac{c_1 y}{x^2+y^2} - c_2 y, -\frac{c_1 x}{x^2+y^2} + c_2 x\Big), \quad (x,y) \in \overline{\Omega}\backslash D, \tag{4.4}$$

and the vorticity

$$\omega = \Delta\psi = -2c_2. \tag{4.5}$$

For any $0 < R_0 < 1$, the functions (4.2) and (4.3) satisfy problem (2.2a), (2.2b), (2.6)-(2.8), with

$$\boldsymbol{f}(x,y) = (c_1 - c_2)(y,-x) = V(-y,x), \qquad (x,y) \in \partial\Omega, \tag{4.6a}$$

$$\boldsymbol{g}(x,y) = \frac{2VR_0^2}{1-R_0^2}(-y,x), \qquad (x,y) \in \partial\Omega, \tag{4.6b}$$

$$p_0 = 0, \qquad \psi_{\partial\Omega} = -\frac{c_2}{2}, \tag{4.6c}$$

$$\psi_{\partial D} = -\frac{1}{2}\left\{c_1 \log(R_0^2) - c_2 R_0^2\right\}, \tag{4.6d}$$

provided

$$c_1 = \frac{VR_0^2}{1-R_0^2}, \quad \text{and} \quad c_2 = \frac{V}{1-R_0^2}, \tag{4.7}$$

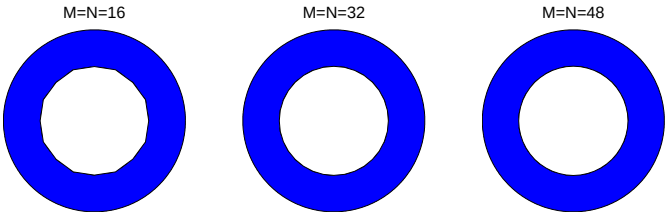

(a) No noise

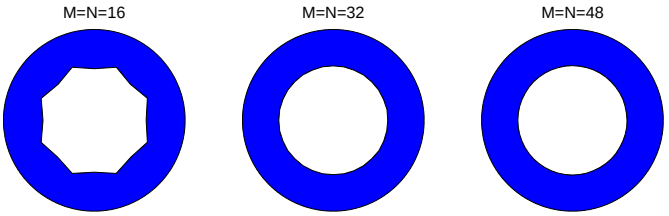

(b) Noise 1%

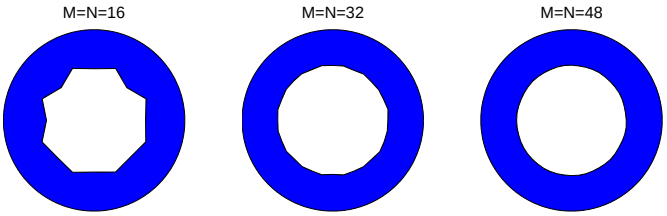

(c) Noise 5%

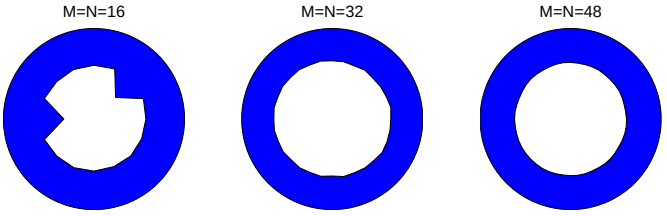

(d) Noise 10%

Figure 2: Results with no regularization and `maxfev=50000` for Example 1.

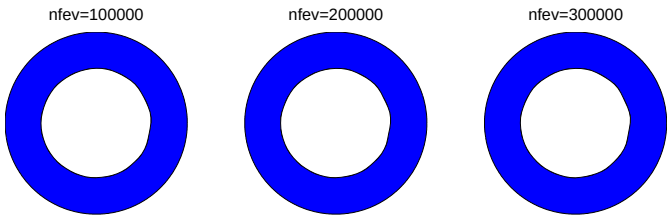

Figure 3: Results with no regularization for Example 1 with $N = M = 64$, with noise 10% for various numbers of function evaluations.

where V is a constant, typically taken to be unity. As one would expect, larger obstacles (with R_0 large) are easier to detect than smaller obstacles (with R_0 small). This

example is also physical as it describes the steady incompressible Stokes flow between two co-axial infinitely long circular cylinders, see [10], in which the inner cylinder D is fixed while the outer cylinder Ω is rotating with constant angular velocity V. In our numerical experiments we choose $V = 1$.

In Figs. 2(a)-2(d), we present the recovered contours obtained with no regularization, i.e.,

$$\lambda_1 = \lambda_2 = 0,$$

in (3.11), for noise levels of $\varepsilon = 0, 1\%, 5\%, 10\%$, respectively, for

$$\texttt{maxfev} = 50000, \quad \text{and} \quad N = M = 16,\ 32,\ 48.$$

As expected, as the level of noise increases, the recovered contours deteriorate. This is very clear for N=M=16, but as M=N increases this feature becomes less distinguishable. In Fig. 3, we present the recovered contours obtained with $N = M = 64$, for a noise level of $\varepsilon = 10\%$ and $\texttt{nfev} = \{1, 2, 3\} \times 10^5$. We observe that increasing nfev has little effect on the recovered solution. Furthermore, the reason for which one does not need to use regularization can be attributed to the fact that in Example 1 a simple circular shape (starting from a similar circular initial guess) is to be retrieved. The next two examples consider retrieving more complicated shapes for which the instability of the solution will be more visibly manifested.

4.2 Example 2

In this example we consider the more complicated kite-shaped domain D with its boundary ∂D given by the radial parametrization

$$r(\vartheta) = \frac{1}{3.5}\sqrt{(-0.25 + 1.3\cos\vartheta + 0.5\cos 2\vartheta)^2 + 2.25\sin^2\vartheta}, \quad \vartheta \in [0, 2\pi). \tag{4.8}$$

The Dirichlet fluid velocity boundary data (1.1c) on $\partial\Omega$ is taken as, see [22],

$$\boldsymbol{u}(x, y) = \boldsymbol{f}(x, y) = \frac{3.5}{12}(y, x), \quad (x, y) \in \partial\Omega = \partial B(0, 1). \tag{4.9}$$

Since in this case no analytical solution is available, the Neumann stress force data (1.1d) on $\partial\Omega$ is simulated by solving the direct problem for the streamfunction ψ and the pressure p given by Eqs. (2.2a), (2.2b), (2.6) with $p_0 = 0$, (2.7a) with $\boldsymbol{f}$ given by (4.9), (2.7c), (2.8a) with $\psi_{\partial\Omega} = 0$, and (2.8b) with $\psi_{\partial D} = 0$, when ∂D is given by (4.8), using the MFS with $M = N = 96$. In order to avoid committing an inverse crime, the inverse solver is applied using a different number $M = N = 64$ and these numbers of source and boundary collocation points are kept fixed in all the remaining figures. Furthermore, noise is added as in (3.14).

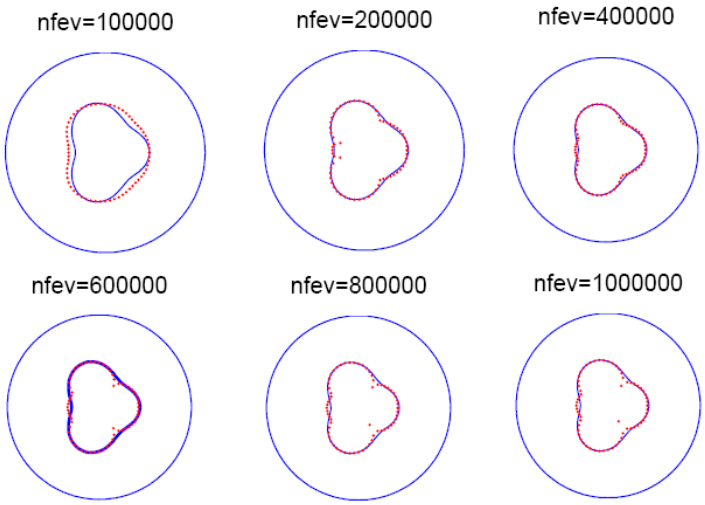

Figure 4: Results for Example 2, with no noise and no regularization for various numbers of function evaluations.

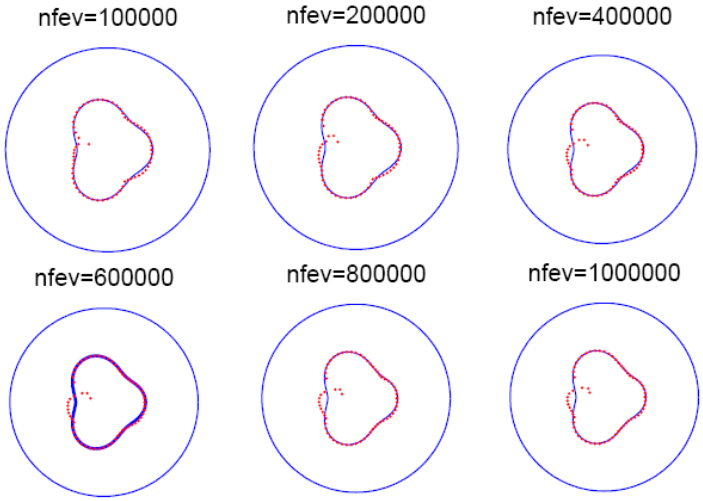

Figure 5: Results for Example 2, with noise 5% and no regularization for various numbers of function evaluations.

In Figs. 4 and 5 we present the numerical results obtained for various numbers of function evaluations with no noise and noise $\varepsilon = 5\%$, respectively, and no regularization. From these figures it can be seen that the most accurate results are obtained for

$$\begin{aligned} &\texttt{nfev} = 4 \times 10^5, \quad \text{for} \quad \varepsilon = 0, \\ &\texttt{nfev} = 10^5, \quad \text{for} \quad \varepsilon = 5\%, \end{aligned}$$

although for other values of `nfev` the results are still reasonable. It appears that the number of function evaluations `nfev`, at which the iteration process should be termi-

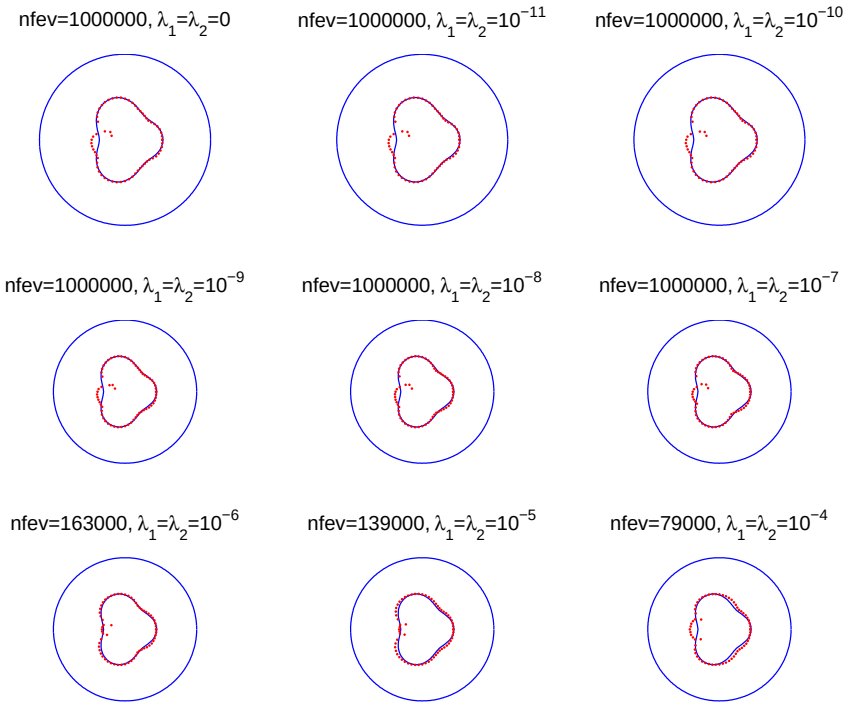

Figure 6: Results for Example 2, with noise 5% and various levels of regularization. The maximum number of function evaluations was set to $\texttt{maxfev} = 10^6$, and, as illustrated, in some cases convergence was reached for a lower number of $\texttt{nfev}$.

nated, plays the role of the regularization parameter. Thus it seems that the iterative minimization procedure employed possesses a regularizing character. That is, if the iterative process is stopped too early then the numerical solution is over smooth, see e.g., Fig. 4 for $\texttt{nfev} = 10^5$, whilst if it is stopped too late then the numerical solution becomes unstable, see Fig. 5 for $\texttt{nfev} = 10^6$. The compromised, i.e., neither too small nor too large, suitable $\texttt{nfev}_{\texttt{opt}}$ at which the iterative process should be terminated depends on the amount of noise ε introduced in the input data (3.14), and, as expected, the value of $\texttt{nfev}_{\texttt{opt}}$ decreases as ε increases. Another way to stabilize the numerical solution is to include regularization in the functional (3.11); however, as shown in Fig. 6, this appears to have little effect on improving the results of Fig. 5.

4.3 Example 3

We finally consider a bean-shaped cavity D with its boundary ∂D given by the radial parametrization

$$r(\vartheta) = \frac{1.4 + 1.26\cos\vartheta + 0.14\sin 2\vartheta}{3.5 + 2.625\cos\vartheta}, \quad \vartheta \in [0, 2\pi). \tag{4.10}$$

Figure 7: Results for Example 3, with no noise and no regularization for various numbers of function evaluations.

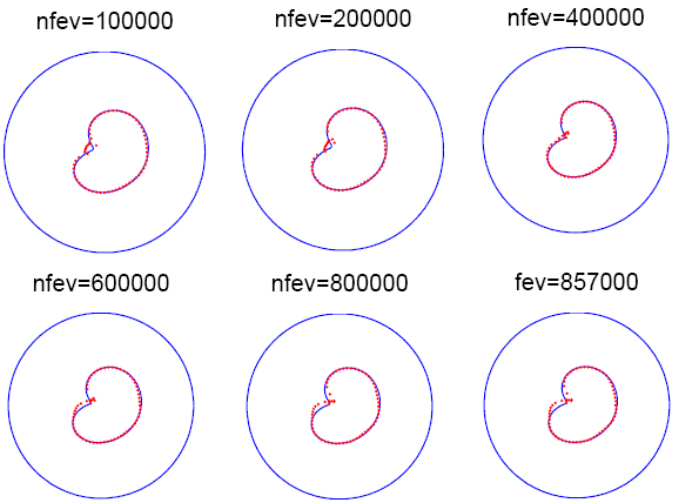

Figure 8: Results for Example 3, with noise 5% and no regularization for various numbers of function evaluations.

This example, which was also considered in [22], is more difficult than the previous two examples because of the presence of a sharp cusp-like portion mimicking a re-entrant corner. The same Dirichlet data (4.9) was taken and all the numerical details are the same as in Example 2. Figs. 7-9 are the analogue of Figs. 4-6, and the same conclusions can be drawn from these. Furthermore, the numerical results we obtained are in good agreement with those of [22].

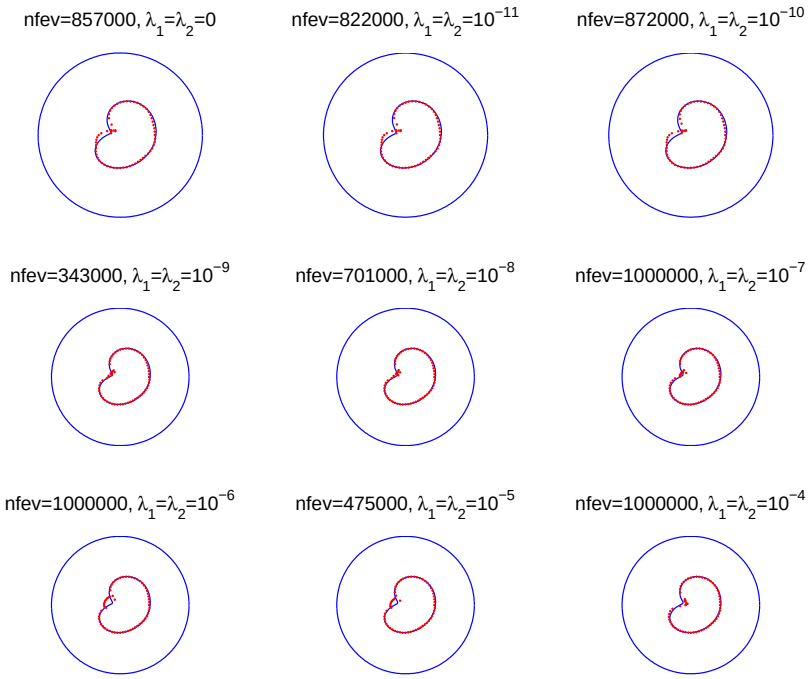

Figure 9: Results for Example 3, with noise 5% and various levels of regularization. The maximum number of function evaluations was set to $\texttt{maxfev} = 10^6$, and, as illustrated, in some cases convergence was reached for a lower number of `nfev`.

5 Conclusions

A novel iterative numerical method based on a regularized MFS has been developed for the approximate solution of the inverse obstacle problem for the Stokes equations in the pressure-streamfunction formulation. The numerical results indicate that accurate and stable reconstructions of the obstacle immersed in the fluid flow can be produced with the proposed method. The extension of the pressure-vectorial streamfunction MFS formulation to three-dimensions is also possible using the Helmholtz decomposition theorem, as described in [25]. However, the inverse analysis becomes more tedious and expensive and is deferred to a future numerical implementation. Possible areas of future research related to the technique presented in this study include the detection of multiple and non-smooth obstacles, and multi-phase flows with unknown interfaces.

Acknowledgements

The authors would like to thank the University of Cyprus for supporting this research. The authors are also grateful to the three anonymous referees for their constructive comments.

References

[1] G. ALESSANDRINI, A. MORASSI AND E. ROSSET, *Detecting cavities by electrostatic boundary measurements*, Inverse Problems, 18 (2002), pp. 1333–1353.

[2] C. ALVAREZ, C. CONCA, L. FRIZ, O. KAVIAN AND J. H. ORTEGA, *Identification of immersed obstacles via boundary measurements*, Inverse Problems, 21 (2005), pp. 1531–1552.

[3] C. ALVAREZ, C. CONCA, R. LECAROS AND J. H. ORTEGA, *On the identification of a rigid body immersed in a fluid: A numerical approach*, Eng. Anal. Bound. Elem., 32 (2008), pp. 919–925,

[4] C. J. S. ALVES, R. KRESS AND A. L. SILVESTRE, *Integral equations for the solution of an inverse boundary value problem for the two-dimensional Stokes equations*, J. Inverse Ill-Posed Probl., 15 (2007), pp. 1–20.

[5] C. J. S. ALVES AND N. F. M. MARTINS, *Reconstruction of inclusions or cavities in potential problems using the MFS*, The Method of Fundamental Solutions - A Meshless Method, (eds. C. S. Chen, A. Karageorghis and Y. S. Smyrlis), Dynamic Publishers, Inc., Atlanta, 2008, pp. 51–73.

[6] C. J. S. ALVES AND N. F. M. MARTINS, *The direct method of fundamental solutions and the inverse Kirsch-Kress method for the reconstruction of elastic inclusions or cavities*, J. Integral Equations Appl., 21 (2009), pp. 153–178.

[7] A. BOGOMOLNY, *Fundamental solutions method for elliptic boundary value problems*, SIAM J. Numer. Anal., 22 (1985), pp. 644–669.

[8] D. BORMAN, D. B. INGHAM, B. T. JOHANSSON AND D. LESNIC, *The method of fundamental solutions for detection of cavities in EIT*, J. Integral Equations Appl., 21 (2009), pp. 381–403.

[9] S. CHRISTIANSEN AND P. HOUGAARD, *An investigation of a pair of integral equations for the biharmonic problem*, J. Inst. Math. Appl., 22 (1978), pp. 15–27.

[10] A. E. CURTEANU, L. ELLIOTT, D. B. INGHAM AND D. LESNIC, *Laplace decomposition and the boundary element method for solving Stokes problems*, Eng. Anal. Bound. Elem., 31 (2007), pp. 501–513.

[11] A. DOUBOVA, E. FERNANDEZ-CARA AND J. H. ORTEGA, *On the identification of a single body immersed in a Navier-Stokes fluid*, European J. Appl. Math., 18 (2007), pp. 57–80.

[12] Z. GAO, Y. MA AND H. ZHUANG, *Shape optimization for Stokes flow*, Appl. Numer. Math., 58 (2008), pp. 827–844.

[13] B. S. GARBOW, K. E. HILLSTROM AND J. J. MORÉ, MINPACK Project, Argonne National Laboratory, 1980.

[14] H. HECK, G. UHLMANN AND J.-N. WANG, *Reconstruction of obstacles immersed in an incompressible fluid*, Inverse Probl. Imaging, 1 (2006), pp. 63–76.

[15] M. S. INGBER AND J. LI, *Surface pressure solution for boundary element analysis of Stokes flow*, Commun. Appl. Numer. Methods, 7 (1991), pp. 367–376.

[16] M. A. JASWON, *Integral equation methods in potential theory, I*, Proc. Roy. Soc. Ser. A 275 (1963), pp. 23–32.

[17] A. KARAGEORGHIS AND G. FAIRWEATHER, *The method of fundamental solutions for the numerical solution of the biharmonic equation*, J. Comput. Phys., 69 (1987), pp. 434–459.

[18] A. KARAGEORGHIS AND G. FAIRWEATHER, *The Almansi method of fundamental solutions for solving biharmonic problems*, Internat. J. Numer. Methods Engrg., 26 (1988), pp. 1665–1682.

[19] A. KARAGEORGHIS AND G. FAIRWEATHER, *The simple layer potential method of fundamental solutions for certain biharmonic problems*, Internat. J. Numer. Methods Fluids, 9 (1989), pp.

1221–1234.

[20] A. KARAGEORGHIS AND D. LESNIC, *Detection of cavities using the method of fundamental solutions*, Inverse Probl. Sci. Eng., 17 (2009), pp. 803–820.

[21] R. KRESS AND S. MAYER, *An inverse boundary value problem for the Oseen equation*, Math. Methods Appl. Sci., 23 (2000), pp. 103–120.

[22] N. F. M. MARTINS AND A. L. SILVESTRE, *An iterative MFS approach for the detection of immeresed obstacles*, Eng. Anal. Bound. Elem., 32 (2008), pp. 517–524.

[23] R. A. MERIC, *An optimization approach for Stokes flow in a channel with a cylindrical block by the BEM*, Eng. Anal. Bound. Elem., 19 (1997), pp. 89–95.

[24] Numerical Algorithms Group Library Mark 21, NAG(UK) Ltd, Wilkinson House, Jordan Hill Road, Oxford, UK, (2007).

[25] J. T. WU AND D. L. YOUNG, Method of Fundamental Solutions for Stokes Problems by the Pressure-Streamfunction Formulation, APCOM'07 in conjunction with EPMESX XI, December 3-6, 2007, Kyoto, Japan, preprint.

[26] W. YAN AND Y. MA, *Shape reconstruction of an inverse Stokes problem*, J. Comput. Appl. Math., 216 (2008), pp. 554–562.